

# Axial Ratio Bandwidth Enhancement of Asymmetrically Fed Microstrip Antenna

Kollannore U. Sam\* and Parambil Abdulla

**Abstract**—Wide axial ratio bandwidth is imparted by placing rigorously designed radial slits on an asymmetrically fed circular radiating patch antenna with parallel bilateral truncations. A partial ground plane with beveling on both the upper corners and a double stepped notch embedded on it makes the antenna suitable for ultra-wideband and X-band applications. The antenna exhibits a  $-10$  dB impedance bandwidth of 8.6 GHz from 3.4 GHz to 12 GHz (111.6%) and a 3 dB axial ratio bandwidth of 8.7 GHz from 3.3 GHz to 12 GHz (113.7%) thereby contributing an effective operating bandwidth of 8.6 GHz (111.6%). The prototype manifests an exceptional far-field radiation pattern and fair gain throughout the passband.

## 1. INTRODUCTION

Reliable wireless communication seldom depends on circularly polarized antennas. As they are insensitive to antenna orientations and have the capability to avoid multipath fading, circularly polarized antennas have been extensively used over linearly polarized antennas [1]. Even after around two decades of the official declaration of 3.1 GHz–10.6 GHz frequency range for ultra-wideband (UWB) by Federal Communication Commission, the increasing demand of the said band attracts the researchers to extend their work on UWB antennas. The X-band is widely used for satellite and terrestrial communication. Antennas exhibiting circular polarization (CP) in those bands is a real breakthrough in implementing novel technologies in wireless communication. The portability of these wireless communication gadgets greatly depends on the antenna profile. Microstrip patch antennas making use of thin planar substrates can be used in transmitter and receiver modules for miniaturization. Individual antennas providing wideband CP avoids the task of fabricating multiple antennas for each specific applications. Single port and dual port feed arrangements with innovative design techniques experimented on the radiator, the ground and the feed are reported to make the antenna exhibit CP. The virtue of CP is judged by its axial ratio (AR) values. The various methods to widen the axial ratio bandwidth (ARBW) may include L-strips on the ground plane [2], single feed asymmetric radiator [3], L-shaped slot and strip [4], horizontal slit and inverted L-strip on the ground [5], L-shaped slot and asymmetric partial ground plane [6], quadrilateral shaped radiating copper with a step-impedance resonator in the feed line [7], and truncated circular radiator with asymmetric feed [8]. A printed monopole antenna loaded with a split ring resonator and a metallic reflector to generate wideband CP behaviour is proposed in [9]. A microstrip antenna embedded with a rotated elliptical slot is detailed in [10]. Numerous works on slot antennas are also reported to achieve wide ARBW [11–20]. None of those antennas could achieve a fractional ARBW of 90% and more. A reformed L-shaped radiating patch connected with inverted-L grounded strip via a tapered slot referred in [21] attains a fractional ARBW of 90.02%. A microstrip

---

*Received 6 May 2020, Accepted 2 June 2020, Scheduled 14 June 2020*

\* Corresponding author: Kollannore Ukkuru Sam (samkoll.mes@gmail.com).

The authors are with the Division of Electronics, School of Engineering, Cochin University of Science and Technology, Kochi-22, Kerala, India.

slot antenna with asymmetric feed presenting an ARBW of 7.3 GHz and a fractional ARBW of 96.7% is proposed in [22].

Circular polarization can be achieved by providing two perturbations placed at diametrically opposite sides on a circular patch [23]. This concept has been adopted in the proposed work wherein only a single truncation is placed on one side of the circular patch to compensate for dual perturbations. Moreover, the area of truncation is made equal to that of the total area of both the perturbations, thereby transforming the circular shape into an approximate semicircular one. The motivation behind this exertion is the keen concern to develop a microstrip patch antenna that could exhibit circular polarization in the whole UWB spectrum and its possible extension, together with the challenge of achieving a 100% axial ratio bandwidth. In this proposed work, an asymmetric feed circular patch with parallel dissimilar bilateral truncations is used as the radiator. Seven radial slits of different depth and width are placed around the radiator to enhance the axial ratio bandwidth. A partial ground plane with beveling on its upper corners and a small rectangular cut at its centre improve the impedance bandwidth. A double stepped notch on one side of the partial ground helps to curtail the value of the axial ratio. The proposed antenna showcases a fractional impedance bandwidth of 111.6% and fractional axial ratio bandwidth of 113.7% with an adequate gain over the entire passband.

## 2. ANTENNA DESIGN AND CONFIGURATION

The proposed antenna has been evolved from our earlier work [8] which has been designed on a circular shaped radiator developed on FR4 substrate, with two parallel dissimilar truncations, chipped on its either side. The primary design equation of the proposed antenna is based on the formula for radius  $r$  of circular microstrip antenna as given in Eqs. (1) and (2) [24].

$$r = \frac{F}{\left[1 + \frac{2h}{\pi\epsilon_r F} \left[\ln\left(\frac{\pi F}{2h}\right) + 1.7726\right]\right]^{1/2}} \tag{1}$$

$$\text{where } F = \frac{8.791 \times 10^9}{f_r \sqrt{\epsilon_r}} \tag{2}$$

A minor segment circle has been truncated from one of its sides to initiate circular polarization. The schematic layout of the basic circular patch with the placement of the said truncation is referred to in Figure 1. The equation for the length of this major truncation,  $T$  is adopted from [8] and is defined in Eq. (3). The distance from the centre of the circle in  $+x$  direction towards the truncation is denoted as  $t1$  and is deduced in Eq. (4). A minor parallel truncation is placed on the other side of the circular patch at a distance  $t2$  from the centre of the patch in  $-x$  direction. This minor truncation will enhance the circular polarization. The radiating patch is fed with an asymmetric feedline having an offset distance

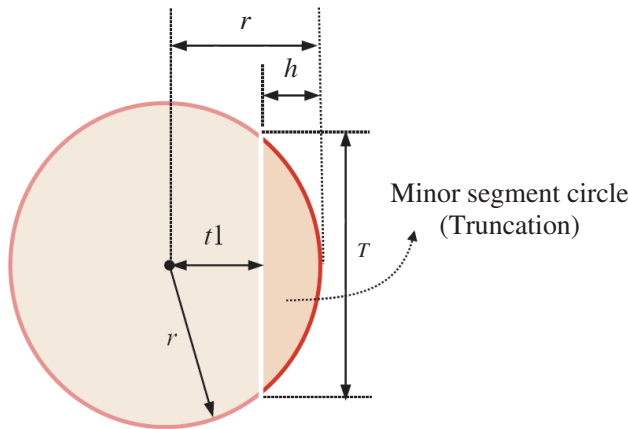


**Figure 1.** Schematic layout of the basic circular radiating patch with the major truncation.

of  $t_3$  in the  $+x$  direction from the centre of the radiator. The asymmetric feed line and the major truncation are the vital elements which invoke circular polarization in the given band of frequencies. Impedance bandwidth of the antenna has been improved by providing symmetrical beveling on both the upper corners of the partial ground plane. A narrow rectangular area has been sheared-off from the top centre portion of the partial ground plane to increase the impedance matching. Seven radial slits of different depth and outer width are placed at different angles along the border of the bilaterally truncated radiator.

$$T = 2\sqrt{2rh - h^2} \tag{3}$$

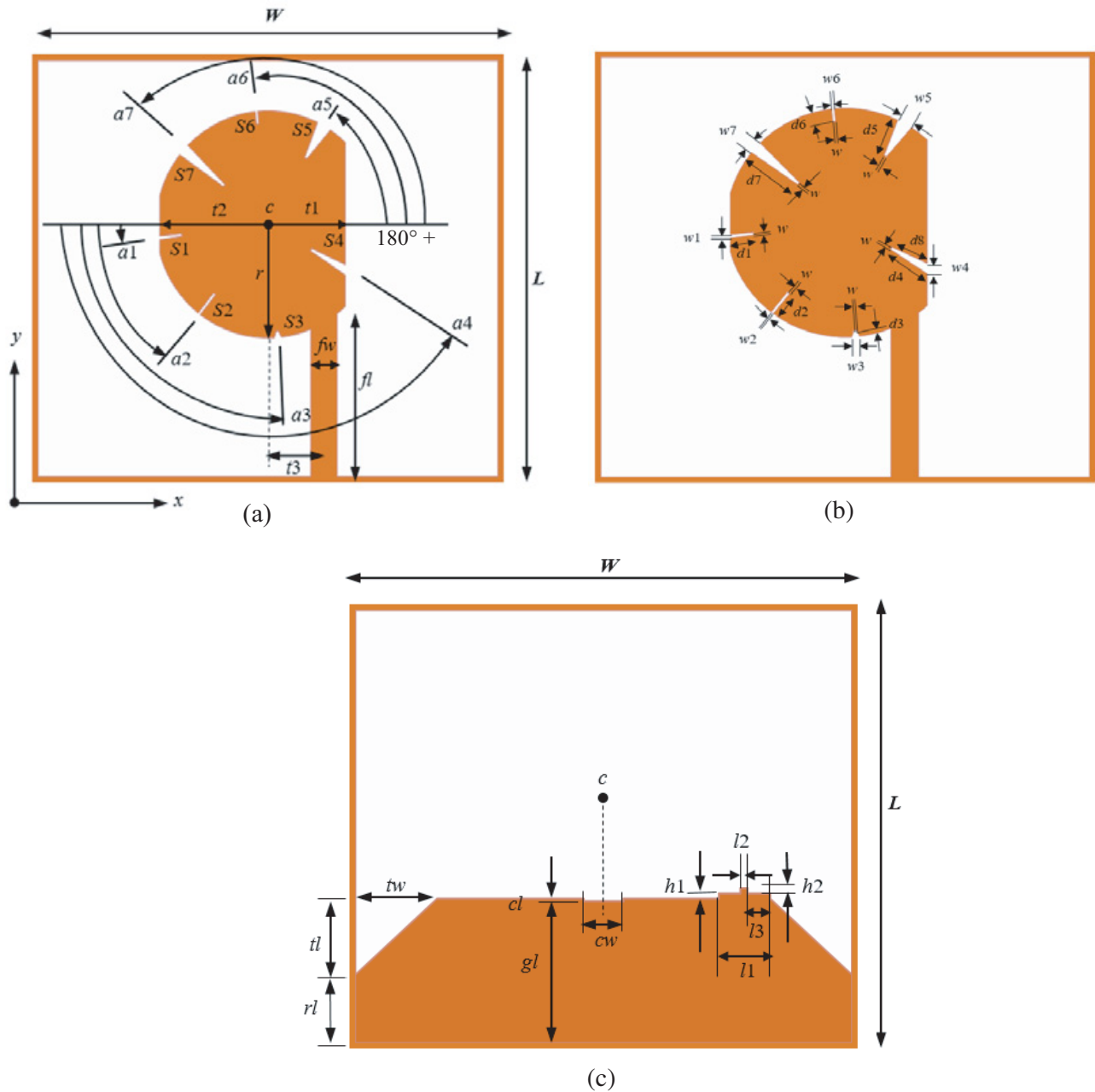


**Figure 2.** The geometrical layout of the proposed antenna. (a) Top view: overall dimensions, (b) top view: patch details and (c) bottom view: partial ground details.

$$t1 = \sqrt{\left(r + \frac{T}{2}\right) \left(r - \frac{T}{2}\right)} \quad (4)$$

The design equation for the placement of the slits is based on multiples of  $45^\circ$ . Placement angle of slit ' $S_n$ ' is denoted as

$$\left. \begin{aligned} an &= (n - 1) \times 45^\circ; & \text{for } n &= 1, 2, 3, 4 \text{ and} \\ an &= n \times 45^\circ; & \text{for } n &= 5, 6, 7. \end{aligned} \right\} \quad (5)$$

Initially, the slits  $S_1$ ,  $S_3$ , and  $S_6$  are placed near  $0^\circ$ ,  $90^\circ$ , and  $270^\circ$ , respectively, avoiding the area of major truncation. Additional slits  $S_2$  and  $S_7$  are placed in between the slits  $S_1$  &  $S_3$  and  $S_1$  &  $S_6$ , respectively. Now the slits  $S_4$  and  $S_5$  are positioned opposite to that of  $S_7$  and  $S_2$ , respectively. The inner width of all the seven slits is fixed as 0.2 mm. A double stepped symmetrical notch is placed near to one of the bevelings at the upper side of the ground. The presence of radial slits together with the embedded double-stepped notch in the partial ground significantly enhance the axial ratio bandwidth from 5.05 GHz to 8.7 GHz. A semicircular microstrip antenna with half the area of a circular microstrip antenna has the same resonance frequency as that of a circular microstrip antenna [23]. The proposed antenna has the approximate shape of a semicircular microstrip antenna with around half the area of a circular microstrip antenna. Hence the frequency of resonance chosen for a circular radiator is applicable for the proposed design.

The geometrical layout of the antenna is shown in Figure 2. An FR4 substrate having a relative permittivity of 4.4, loss tangent of 0.02, and an overall dimension of  $37 \times 33 \times 1.6$  mm is used for simulation and fabrication. The thickness of the copper medium is considered as  $0.35 \mu\text{m}$ . Table 1 lists the optimized dimensions of each parameter for achieving maximum ARBW.

**Table 1.** Optimized geometrical parameters of the antenna.

<i>Parameter</i>	<i>Value</i>	<i>Parameter</i>	<i>Value</i>	<i>Parameter</i>	<i>Value</i>	<i>Parameter</i>	<i>Value</i>
<i>L</i>	37 mm	<i>rl</i>	5.2 mm	<i>a1</i>	$7^\circ$	<i>w5</i>	1.2 mm
<i>W</i>	33 mm	<i>tl</i>	5.8 mm	<i>a2</i>	$52^\circ$	<i>w6</i>	0.2 mm
<i>R</i>	9 mm	<i>tw</i>	6.1 mm	<i>a3</i>	$95^\circ$	<i>w7</i>	1.0 mm
<i>H</i>	1.6 mm	<i>cl</i>	0.2 mm	<i>a4</i>	$150^\circ$	<i>d1</i>	1.76 mm
$\epsilon_r$	4.4	<i>cw</i>	3.0 mm	<i>a5</i>	$240^\circ$	<i>d2</i>	1.99 mm
<i>Fl</i>	11.9 mm	<i>h1</i>	0.4 mm	<i>a6</i>	$276^\circ$	<i>d3</i>	0.53 mm
<i>Fw</i>	2.1 mm	<i>h2</i>	0.4 mm	<i>a7</i>	$319^\circ$	<i>d4</i>	3.4 mm
<i>t1</i>	6.2 mm	<i>l1</i>	3.8 mm	<i>w1</i>	0.3 mm	<i>d5</i>	2.97 mm
<i>t2</i>	8.7 mm	<i>l2</i>	0.5 mm	<i>w2</i>	0.2 mm	<i>d6</i>	0.99 mm
<i>t3</i>	4.5 mm	<i>l3</i>	1.65 mm	<i>w3</i>	0.6 mm	<i>d7</i>	4.3 mm
<i>Gl</i>	10.8 mm	<i>w</i>	0.2 mm	<i>w4</i>	0.8 mm	<i>d8</i>	3.38 mm

### 3. RESULTS AND DISCUSSION

Thorough simulations were done using CST Microwave Studio software for obtaining optimized results. Figure 3 shows the prototype of the antenna fabricated on FR4 substrate. The results are measured using Network Analyzer ENA (E 5071C). Unused legs of the SMA connector were removed to avoid the spurious radiations.

#### 3.1. Reflection Coefficient

The reflection coefficient is defined as the figure that estimates the proportion of electromagnetic wave that is reflected by an impedance discontinuity in the transmission medium. Figure 4 illustrates the

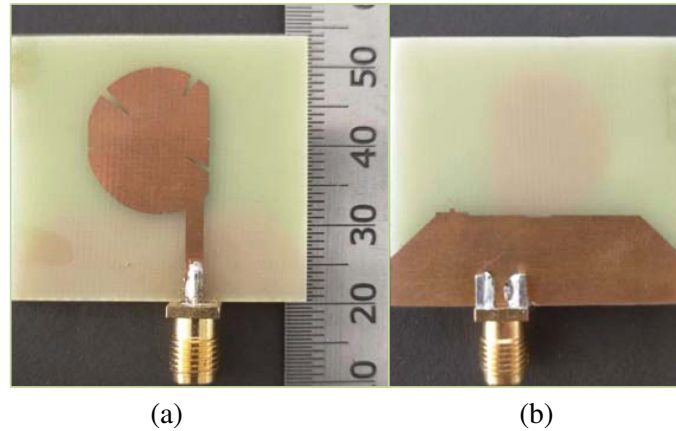


**Figure 3.** The fabricated prototype used for measurements. (a) Top view and (b) bottom view.

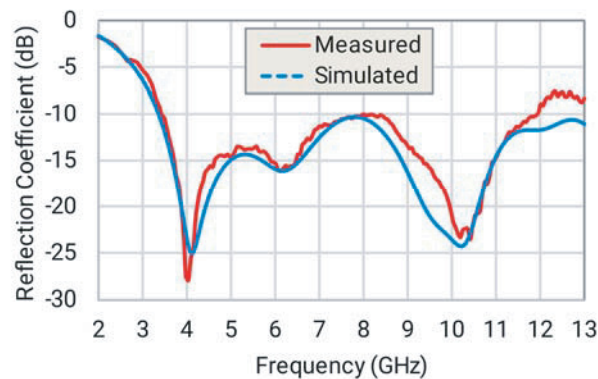


**Figure 4.** Simulated and measured reflection coefficient plots.

simulated and measured reflection coefficient plots. The simulated 10-dB impedance bandwidth has a lower frequency limit of 3.3 GHz and extends over 12 GHz. An impedance bandwidth of 8.6 GHz from 3.4 GHz to 12 GHz is obtained during measurement. Resonances are obtained at 4.04 GHz and around 10.42 GHz. A minor variation of return loss in the higher operating frequencies may be due to the variations on the substrate permittivity at high frequencies. The dielectric constant decreases with increasing frequency of operation. It also decreases with an increase in the resin content (% weight) for a particular frequency of operation [25, 26]. Even the copper thickness was found to be varying between 0.033 mm and 0.0356 mm. As a result, the material variations although not very prominent at lower frequencies become significant at the higher ones and become a major source of performance nonlinearities and degradation. The frequency bands that are enclosed by the proposed antenna may include the whole C-band (4–8 GHz), the X-band (8–12 GHz) and the UWB (3.1–10.6 GHz) with a short of 0.2 GHz.

Parametric studies are carried out to investigate the effect of placement of asymmetric microstrip feed ( $t_3$ ) on the reflection coefficient of the antenna. The curves plotted in Figure 5(a) conveys that the positioning of the microstrip feed line has a substantial role in complimenting the impedance of the antenna. The variation of the reflection coefficient is at par with the placement of feedline till 9 GHz, afterwards it is assumed that the dielectric constant of the substrate comes into the picture and hence the reflection coefficient characteristics may depend on it and varies correspondingly. A similar analysis is carried on the depth of the rectangular cut ( $cl$ ) which is centrally placed on the upper part of the partial ground. Traces plotted in Figure 5(b) reveals that the effect of varying the depth of the rectangular cut is to shift the reflection coefficient of the entire band without any change in its shape, except in the lower frequencies where it has no effects. Even though the antenna exhibits excellent

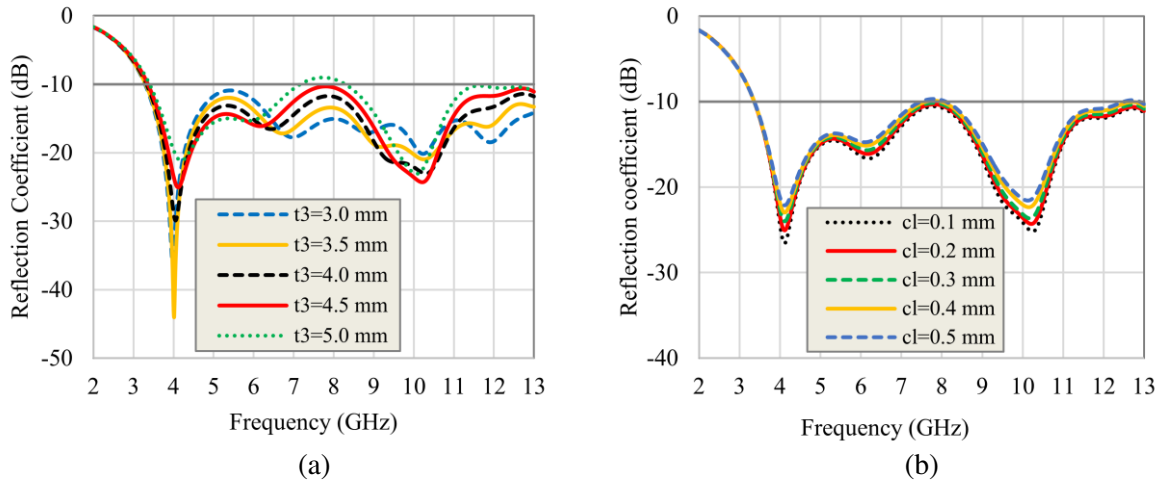


**Figure 5.** Parametric measurements on reflection coefficients. (a) Variation with feed line offset,  $t_3$  and (b) variation with the depth of rectangular cut,  $cl$  in the partial ground.

matching of impedance at  $t_3 = 3.5$  mm and  $cl = 0.1$  mm, we choose  $t_3 = 4.5$  mm and  $cl = 0.2$  mm for achieving good axial ratio and fair gain.

### 3.2. Axial Ratio

Antennas radiate circularly polarized waves when excited by two orthogonal field components with equal amplitude and in phase quadrature. The principal elements employed for manifesting wideband circular polarization in this proposed antenna design are

- i) Asymmetric feed line
- ii) Truncations on the circular patch
- iii) Slits on the radiator and
- iv) Double stepped notch on the partial ground.

The purity of circular polarization is evaluated by its axial ratio value which is the ratio between the minor and major axis of the polarization ellipse. Ideally, an antenna is said to be circularly polarized when its axial ratio attains unity (or 0 dB), wherein the polarization ellipse has an equal minor and major axis and transforms into a circle. In that case, the axial ratio is equal to unity. A linearly polarized antenna will have infinitely large axial ratio since one of the axes of the ellipse is equal to zero. For a circularly polarized antenna, the closer the axial ratio is to 0 dB, the better the purity of circular polarization. Figure 6 depicts the simulated and measured axial ratio plots. The antenna exhibits circular polarization from 3.3 GHz to 12 GHz providing an ARBW of 8.7 GHz in its measured result. Simulated 3-dB axial ratio plot almost resembles with the measured one throughout the entire frequency band, except at the higher end of the passband where the measured result shows a short of 0.8 GHz in its ARBW. Inaccuracies in the fabrication of the antenna prototype, particularly in the positioning of the feed line and the major truncation are the primary cause for the early rise of the measured curve from its simulated one. Table 2 tabulates a few simulated and measured near-to-zero values of AR. The minimum value of axial ratio attained by the proposed antenna in the simulation and measurement is 0.018 dB (at 11.55 GHz) and 0.3 dB (at 6.01 GHz) respectively. There are few instances in which the measured AR plot just grazes the 3 dB line. These unexpected variations are probably due to the minor fabrication tolerances on the depth of slits  $S_5$  and  $S_7$ .

The classic method to initiate circular polarization in a microstrip antenna is by introducing asymmetric feed line. The length, width and positioning of the asymmetric feed line along with the diameter of the circular patch, determine the depth of the CP and the frequencies at which the antenna exhibit CP. Orthogonal field components are generated by instigating an offset distance for the feed line or by chipping the sides of the circular patch by dissimilar parallel truncations. The

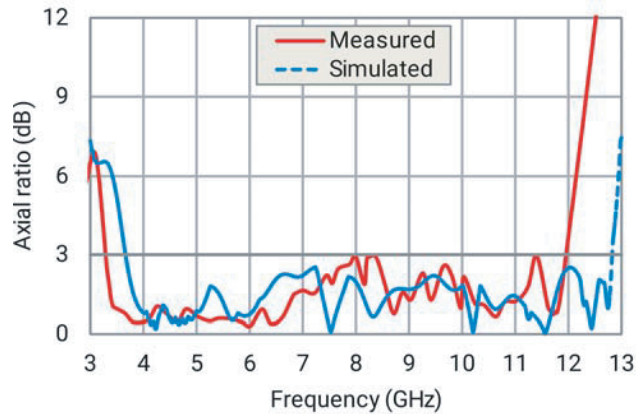


**Figure 6.** Simulated and measured axial ratio plots.

**Table 2.** Typical simulated and measured AR values.

Simulated		Measured	
AR value (dB)	Frequency (GHz)	AR value (dB)	Frequency (GHz)
0.200	4.23	0.44	3.81
0.100	7.52	0.3	6.01
0.111	10.19	0.76	8.71
0.018	11.55	0.64	10.63
0.203	12.44	0.79	11.73

asymmetric feed, even without any truncation can develop an electrical difference in the diameter of the patch. Similarly, the dissimilar truncations even without asymmetric feed can develop both electrical and physical difference in the diameter of the radiating circular patch in the directions of  $x$  and  $y$ -axis. These features are characterized and analyzed in our earlier work [8] where a total axial ratio bandwidth of 5.05 GHz spread over two bands was reported. The deviations in the mid-range frequencies are attributed by the slight inaccuracies in the placement of the feed line, which is verified by the parametric traces plotted in Figure 7(a). Shifting of the feed line away from the central position towards  $+x$  direction reduces the value of axial ratio till it reaches a lowest average value at  $t3 = 4.5$  mm, beyond which it rises again. Variation of axial ratio in accordance with the position of the major truncation  $t1$  and the minor truncation  $t2$  is plotted in Figure 7(b) and Figure 8(a). The plots convey that the major truncation has got the role of course tuning and the minor truncation has got the role of fine-tuning of the axial ratio across the passband of the antenna. Moving the major truncation  $t1$  away from the centre of the patch has the effect of raising the axial ratio in the lower band frequencies and lowering the axial ratio in the upper band. Similarly, moving the major truncation  $t1$  closer to the centre of the patch has the effect of raising the axial ratio in the upper band frequencies and lowering the axial ratio in the lower band. The aftermath of the latter case may be another cause of deviation of axial ratio in the measured curve. The other causes are the non-uniform thickness of the substrate and systematic errors in measurements. The thickness of the FR4 substrate that has been used for the fabrication of the antenna may different compared to its actual value of 1.6 mm. Also, there may be a possibility of uneven thickness of the substrate and the copper film across the surface of the material. Figure 8(b) reveals that minor deformities in the thickness of the substrate will come into the picture and affect the axial ratio beyond 9.5 GHz.

The radial slits on the truncated circular patch further improve the CP bandwidth to achieve value beyond 8 GHz. Apart from the position of truncation and feed line, the other three parameters which are used to vary the axial ratio levels are angular position, depth and outer width of each radial slit.

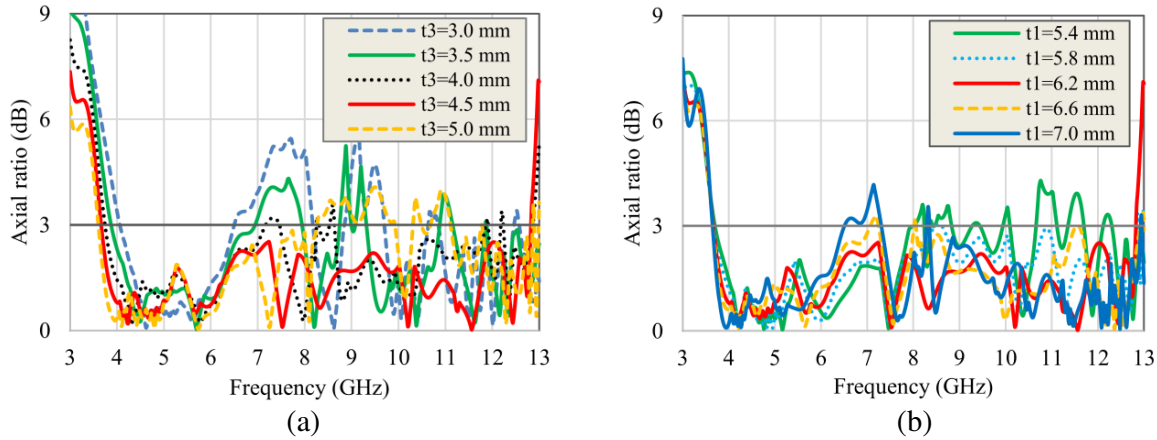


**Figure 7.** Parametric measurements on axial ratio. (a) Variation with feed line offset,  $t_3$  and (b) variation with distance to major truncation,  $t_1$ .

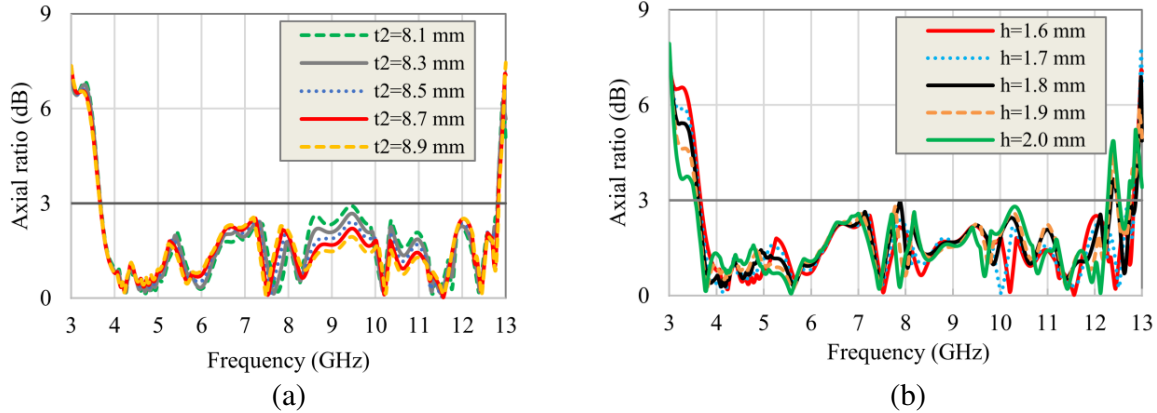


**Figure 8.** Parametric analysis on axial ratio. (a) Variation with distance to minor truncation,  $t_2$  and (b) variation with substrate height,  $h$ .

Final tuning of the 3-dB axial ratio bandwidth in the high-frequency range is done by integrating a double-stepped notch on one half of the partial ground and by adjusting the position, width and height of each step of the notch.

Parametric analysis is carried out to see the effect of dimensions of major slits ( $S_4$ ,  $S_5$  and  $S_7$ ) on the axial ratio viz. angle of placement of  $S_4$  and  $S_7$ , depth of  $S_5$  and  $S_7$  and outer width of  $S_4$  and  $S_5$ . Two out of the three major slits are considered for parametric analysis. The variation on axial ratio by changing the dimensions of minor slits ( $S_1$ ,  $S_2$ ,  $S_3$  and  $S_5$ ) are not included in this article as their effects are less critical on the antenna parameters. Here we have fixed the inner width of the slits as 0.2 mm. Further reduction of the inner width of the slits may improve the purity of circular polarization and axial ratio stability across the whole band of the antenna. But the limitations of fabrication differ us from such procedures. Figure 9 describes that lowering the angle  $a_4$  shifts the axial ratio down towards zero level between the frequency limits 8 GHz and 11 GHz whereas increasing the angle  $a_7$  pull down the axial ratio largely within 10 GHz and 11 GHz. Both the angles do not have a considerable effect in the lower frequencies.

Figures 10(a) and 10(b) depict the outcome of axial ratio in accordance with the variation in depth of slits  $d_5$  and  $d_7$  respectively. Increasing the depth will improve the axial ratio until its optimized design value and afterwards it degrades. The design of depth  $d_5$  has to be done in extreme care, as it affects not only the axial ratio magnitude but also effects the axial ratio bandwidth. The angle  $d_7$  has got wide control over the frequencies from 5 GHz to 13 GHz. One of the reasons for the dominance

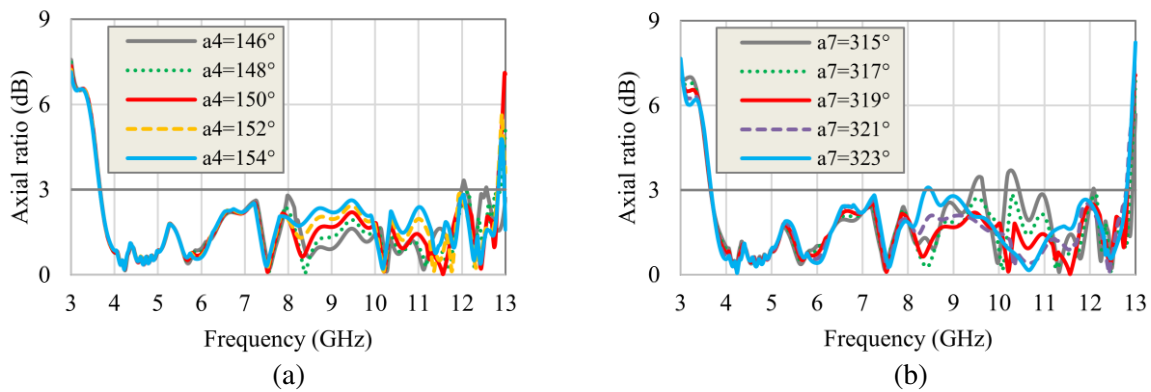


**Figure 9.** Parametric measurements on axial ratio. (a) Variation with the angular position of  $S_4$  and (b) variation with the angular position of  $S_7$ .

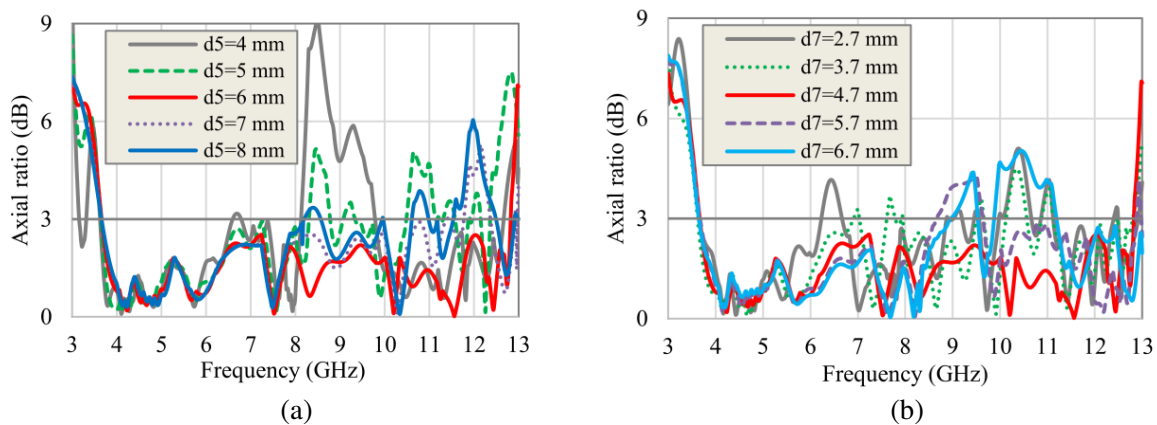


**Figure 10.** Parametric studies on axial ratio. (a) Variation with depth of slit  $S_5$  and (b) variation with depth of slit  $S_7$ .

of  $d_5$  and  $d_7$  on the overall performance of the antenna is that these slits have the maximum outer width. Figures 11(a) and 11(b) convey that varying the value of outer width alone does not have much contributions on the traces of axial ratio, but for different values of outer width, the variation of other parameters will significantly judge the usable bandwidth of operation.

Figure 12(a) not only discloses the result of integrating the partial ground with a different combination of notches but also inculcates a definite direction regarding the choice of selecting the placement of double-stepped notch on the right-hand side (RHS) of the ground. As shown in the graph, the placement of notches on the right-hand side of the partial ground (solid curves) improves the axial ratio than placing the notches on the left-hand side (LHS) of the ground (dotted curves). This is due to the proximity of the notches with the asymmetric feed line and the major truncation. Incorporating the partial ground with stepped notches at the right-hand side drastically improves the axial ratio, particularly between 8.2 GHz–10 GHz and 10.4 GHz–11.5 GHz which is self-explanatory from the traces. Uniformity of the circular polarization is verified by tracing the axial ratio characteristics for different values of  $\phi$ . viz.  $\phi = 0^\circ, 90^\circ, 180^\circ$  and  $270^\circ$ . Figure 12(b) explains that an ARBW of at least 8.3 GHz (4.6 GHz–12.9 GHz) is achieved by considering all the above-mentioned angles of  $\phi$ . The main reason for obtaining a uniform CP throughout the  $\phi$  values is the placement of radial slits in contrapositions. Figure 13 summarizes the effect of various developmental stages of the proposed antenna on its axial ratio. In each stage, the axial ratio and its bandwidth improve significantly.

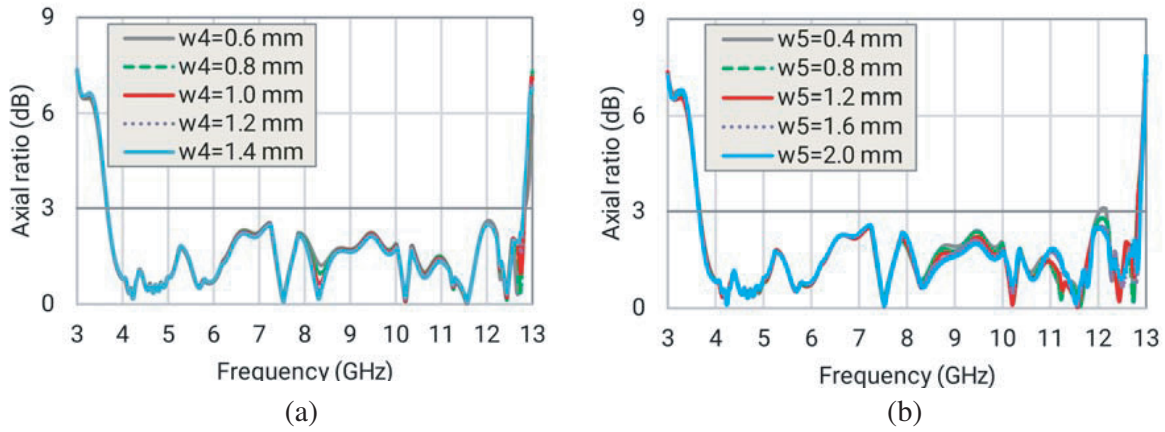


**Figure 11.** Parametric analysis on axial ratio. (a) Variation with the outer width of slit  $S_4$  and (b) variation with the outer width of slit  $S_5$ .

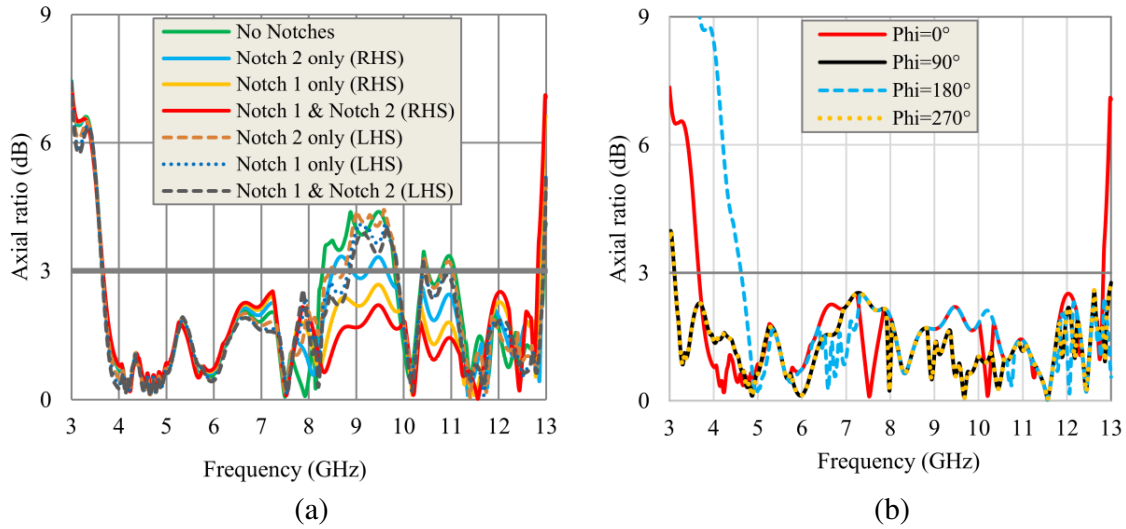


**Figure 12.** Parametric analysis on axial ratio. (a) Variation with various combination of notches and (b) variation with values of phi.

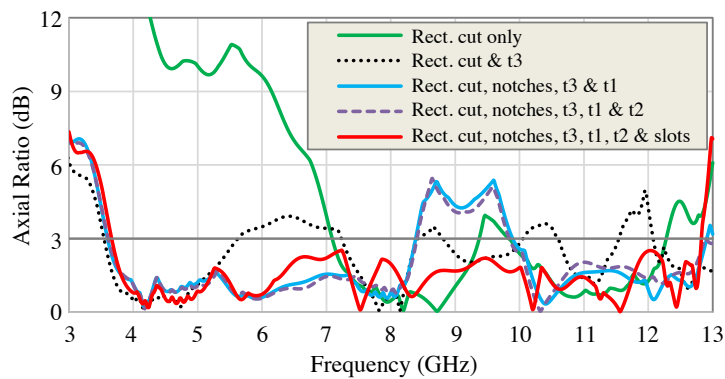


**Figure 13.** Parametric studies on the axial ratio in various stages of development of the proposed antenna.

### 3.3. Sense of Polarization

Sense of the circular polarization can be investigated by verifying the direction of current patterns on the surface of the radiating element. Figures 14, 15 and 16 demonstrate the rotation of surface current pattern at three frequency points (4 GHz, 7.5 GHz and 11 GHz) across the whole operating band of the antenna at various phases viz.  $0^\circ$ ,  $90^\circ$ ,  $180^\circ$  and  $270^\circ$ . It is evident that the simulated current patterns rotate in a clockwise direction when looking towards the paper, hence the proof that the antenna exhibit left-hand circular polarization (LHCP). Since the truncated circular patch without slits produces the same LHCP, it is verified that the sense of circular polarization will not be altered by introducing slits on the radiating surface but its effect is to widen the ARBW.

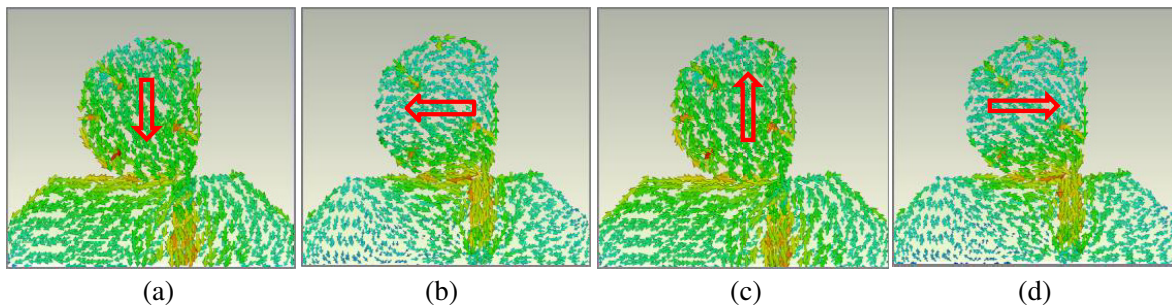


**Figure 14.** Surface current distribution at 4 GHz. (a) Phase =  $0^\circ$ , (b) Phase =  $90^\circ$ , (c) Phase =  $180^\circ$ , and (d) Phase =  $270^\circ$ .

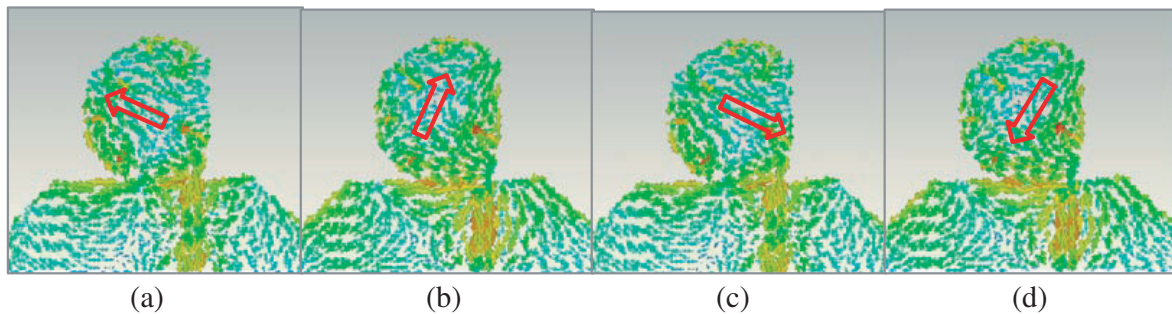


**Figure 15.** Surface current distribution at 7.5 GHz. (a) Phase =  $0^\circ$ , (b) Phase =  $90^\circ$ , (c) Phase =  $180^\circ$ , and (d) Phase =  $270^\circ$ .

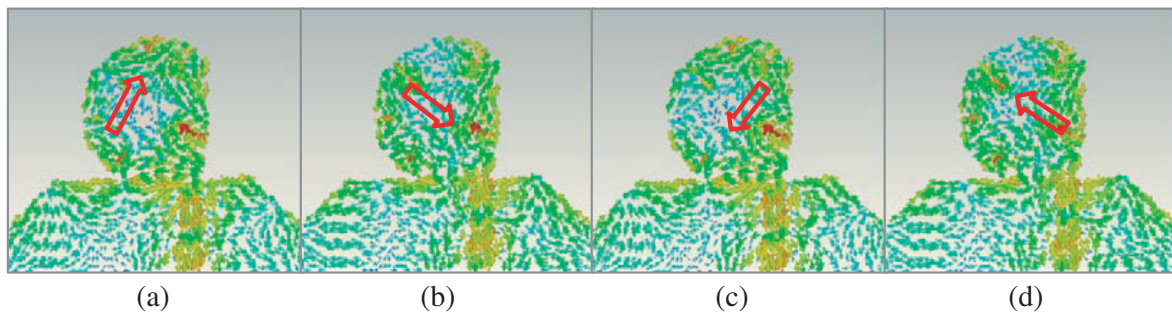


**Figure 16.** Surface current distribution at 11 GHz. (a) Phase =  $0^\circ$ , (b) Phase =  $90^\circ$ , (c) Phase =  $180^\circ$ , and (d) Phase =  $270^\circ$ .

### 3.4. Gain

The extent to which an antenna concentrates the radiated power in a given direction or absorbs incident power from that direction, compared with a reference antenna, is termed as the gain of that antenna. The traces plotted in Figure 17 illustrates the variation in gain across the possible operating frequencies. An attempt has been made to compare the gain of the proposed antenna with the antenna reported in [8]. A measured peak gain of 6.6 dB is obtained at 7 GHz for the antenna without slits and notches. The simulated plots affirm that the gain of the antenna will not be suffered by inserting radial slits. Instead, the gain is improved in between the frequencies 4.2 GHz and 6.8 GHz. Integration of notches on the partial ground never deteriorates the gain, but it emends slightly beyond 11 GHz. The simulated peak gain of 5.59 dB is attained at 11.8 GHz. Other parametric factors which influence the antenna gain are the height of the substrate and the microstrip feed position. Studies have been carried out to investigate the role of the height of the substrate  $h$  and the feed offset position  $t_3$  on the gain of the antenna. Figure 18(a) indicates that the gain of the antenna increases with  $h$  in the frequencies 4.5 GHz–6.4 GHz and 6.8 GHz–10 GHz. The decrease in the gain of the antenna in the upper band may be due to the following possible reasons. The relative permittivity of the FR-4 substrate tends to decrease with increase in frequency [27] and may degrade the gain of the antenna at high frequencies. Besides, with increasing the substrate thickness, the bandwidth increases but the antenna dimensions decreases as well as the centre operating frequency moves away from the desired resonance frequency and thereby reducing the gain at frequencies away from its designed frequency [28, 29]. The decrease in the gain beyond 12 GHz can be neglected as it is not covered under the operating frequency range. Figure 18(b) shows that the feed offset distance  $t_3$  significantly controls the gain of the antenna. Between 4.4 GHz

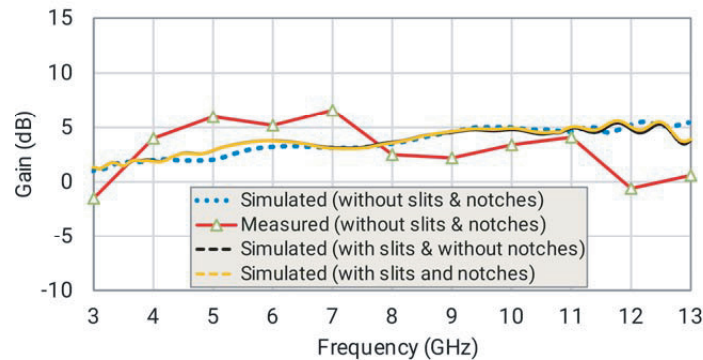


**Figure 17.** Simulated and measured plots of gain.

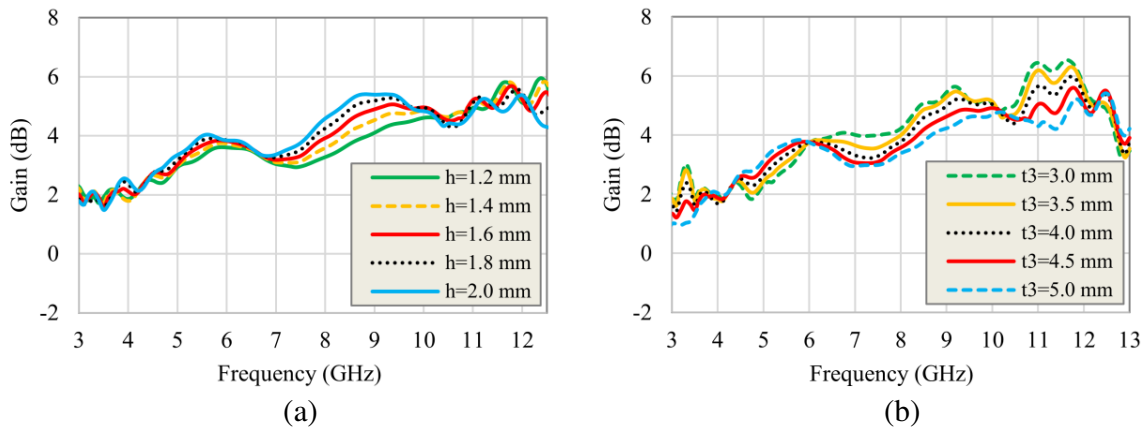


**Figure 18.** Parametric analysis on gain. (a) Variation of gain with the height of the substrate  $h$  and (b) variation with feed line offset  $t_3$ .

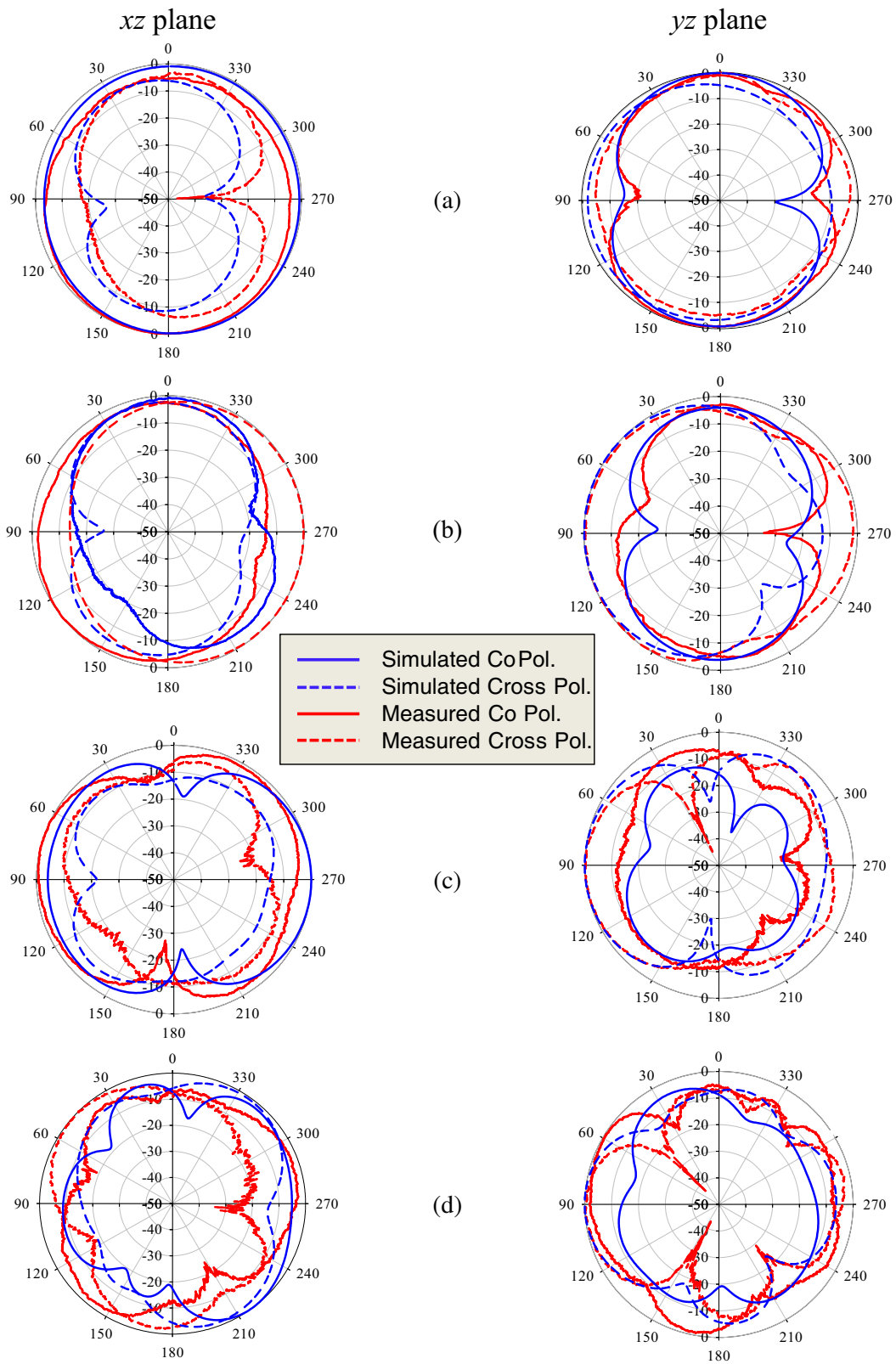


**Figure 19.** Normalized radiation patterns showing co and cross polarizations. (a) 3.88 GHz, (b) 5.14 GHz, (c) 8.8 GHz, and (d) 11.56 GHz.

and 6 GHz, its role is to increase the gain and between 6 GHz and 12 GHz its role is to decrease the gain upon increasing the feed offset distance  $t_3$ . A maximum augment of 2 dB is manifested around 11.4 GHz with a feed line offset of 2 mm from the centre of the patch in the  $+x$  direction.

**Table 3.** Comparison of critical parameters with other reported work.

Ref.	Substrate/ Dimension (mm)	IBW/Band (GHz)	Fractional IBW	ARBW/Band (GHz)	Fractional ARBW	Peak gain (dB)
[2]	FR4: $60 \times 60 \times 0.8$	10.33 (2.67–13)	131.8%	1.952 (4.993–6.945)	32.2%	4.2
[3]	FR4: $28 \times 29 \times 1.6$	7.95 (2.98–10.93)	113.6%	2.83 (7.18–10.01)	33%	Not mentioned
[4]	Rogers RO4003: $20 \times 20 \times 0.813$	2.4 (4.8–7.2)	40%	1.95 (5.15–7.1)	33%	3.6
[5]	FR4: $25 \times 24 \times 1$	4 (4.8–8.8)	58.8%	3.375 (5.375–8.75)	47.8%	3.4
[6]	FR4: $50 \times 50 \times 0.8$	4.82 (2.15–6.97)	105.7%	3.9 (3.1–7)	71%	5
[7]	FR4: $30 \times 25 \times 0.8$	14.4 (3.1–17.5)	139.8%	4.67 (5.91–10.58)	56.64%	5.67
[8]	FR4: $37 \times 33 \times 1.6$	7.6 (3.4–11)	105.5%	5.05 (3.4–7.6) & (8.65–9.5)	85.8%	5.73
[11]	FR4: $44 \times 42 \times 0.8$	2.56 (2.05–4.61)	76.8%	2.41 (2.19–4.6)	71%	2.8
[12]	FR4: $20 \times 20 \times 1.6$	4.6 (4–8.6)	73.0%	3.45 (5–8.5)	51.8%	5
[13]	RT/Duroid 5880: $28 \times 28 \times 1.6$	4.75 (3.25–8)	84.4%	2.27 (4.4–6.67)	41.0%	3
[14]	FR4: $30 \times 30 \times 1.6$	3.79 (2.61–6.4)	84.1%	3.25 (3.1–6.35)	68.7%	3.8
[15]	FR4: Radius = 58.8	5.1 (2.9–8)	93.5%	3 (3–6)	66.6%	4.9
[16]	FR4: $25 \times 25 \times 1.5$	5.3 (3.2–8.5)	90.5%	4.8 (3.3–8.1)	84.2%	3.56
[17]	FR4: $60 \times 60 \times 1.6$	17.1 (2.9–20)	149.3%	2.6 (2.9–5.5)	61.9%	5
[18]	FR4: $25 \times 25 \times 0.8$	12.06 (2.76–14.82)	137.2%	1.86 (4.27–6.13)	35.7%	3.2
[19]	FR4: $68 \times 33 \times 1.6$	13.33 (0.170–13.5)	200%	1.9 (4.9–6.8)	32.5%	4
[20]	FR4: $40 \times 40 \times 1.58$	9.5 (2.5–12)	97.4%	4.4 (3.2–7.6)	81.1%	3.7
[21]	FR4: $40 \times 45 \times 1.5$	5.22 (2.3–7.52)	106.3%	3.7 (2.25–5.95)	90.02%	5.2
[22]	FR4: $30 \times 33.5 \times 0.8$	10.05 (2.55–12.6)	132.6%	7.3 (3.9–11.2)	96.7%	4.1
This work	FR4: $37 \times 33 \times 1.6$	8.6 (3.4–12)	111.6%	8.7 (3.3–12)	113.7%	5.59

### 3.5. Radiation Pattern

Radiation patterns are plotted not only to measure the antenna parameters and to analyze the purity of polarization but also to fix the position of receiving antennas to catch the maximum amount of radiated electromagnetic waves. Normalized co-polarized and cross-polarized radiation patterns in  $yz$  plane and  $xz$  plane at four different frequency locations within the entire passband viz. 3.88 GHz, 5.14 GHz, 8.8 GHz and 11.56 GHz are plotted in Figures 19(a)–(d). Simulated and measured values illustrate the presence of circular polarization in the  $+z$  and  $-z$  axis except in  $-z$  axis ( $\theta = 180^\circ$ ) at 11.56 GHz, where the difference between the co-polarization and cross-polarization levels reach around 10 dB. The patterns reflect a functional beam width (where the difference between the co-polarized and cross-polarized patterns is less than 3 dB) of at least  $60^\circ$  in the  $+z$  axis across the whole band with an exception at 8.8 GHz in the  $yz$  plane which may be due to the tilt in the pattern. Increase in the cross-polar levels is due to the finite size of the partial ground plane placed away from the bottom of the radiator space. The purity of circular polarization and the beamwidth of the radiation pattern improves as approaching towards the lower end of the frequency band.

The minor tilt in the lobe is mainly due to the combined effect of the asymmetric shape of the radiator and the feed line offset. As moving towards high frequencies, a slight amount of pattern fluctuations is observed which may be due to possible measurement errors.

### 3.6. Comparative Studies

The results of the proposed antenna are compared with the values of similar antennas reported in published articles. Table 3 highlights the value of critical radiation parameters of those antennas taken for comparison. The antenna exhibits the widest ARBW (8.7 GHz) among the comparable works. It is prima facie understood that none of the works except the proposed antenna exhibit more than 100% fractional IBW and fractional ARBW. Besides, 100% of its IBW has been transformed to disseminate circular polarization. Inserting the slits reduce the area of the truncated circular radiator by 3.28% (from  $228.19 \text{ mm}^2$  to  $220.8 \text{ mm}^2$ ). But the introduction of the slits along with the integration of double-stepped notches ( $1.72 \text{ mm}^2$ ) in the partial ground improves the ARBW by 72.27% (from 5.05 GHz to 8.7 GHz) [8]. Also, this minor reduction in the size of the radiator did not affect the overall gain of the antenna. The proposed antenna is compact compared to the other reported works.

## 4. CONCLUSION

The design equations for the basic structure of the proposed planar antenna has been developed by the authors in the earlier work and is been adopted here and introduced more design features to enhance the impedance bandwidth and axial ratio bandwidth. This research work deploying asymmetric feed planar antenna exhibits broad impedance bandwidth of 8.6 GHz (3.4 GHz–12 GHz) and wide axial ratio bandwidth of 8.7 GHz (3.3 GHz–12 GHz) which merges the UWB and X band frequencies with a short of only 0.2 GHz in the lower end of UWB. Besides, the antenna manifests an effective fractional axial ratio bandwidth of 111.6%. The antenna presents a fair gain throughout the passband with a peak value of 5.59 dB. Measured radiation patterns display excellent farfield characteristics. The proposed antenna is potentially suitable for applications in UWB, S-band, C-band and X-band frequencies.

## REFERENCES

1. Quan, X., R. Li, and M. M. Tentzeris, "A broadband omnidirectional circularly polarized antenna," *IEEE Transactions on Antennas and Propagation*, Vol. 61, No. 5, 2363–2370, Jan. 2013.
2. Pourahmadazar, J., Ch. Ghobadi, J. Nourinia, N. Felegari, and H. Shirzad, "Broadband CPW-fed circularly polarized square slot antenna with inverted L-strips for UWB applications," *IEEE Antennas and Wireless Propagation Letters*, Vol. 10, 369–372, Apr. 2011.
3. Rahim, S. A., Sh. Danesh, U. A. Okonkwo, M. Sabran, and M. Khalily, "UWB monopole antenna with circular polarization," *Microwave and Optical Technology Letters*, Vol. 54, No. 4, 949–953, Apr. 2012.

4. Ahdi Rezaeieh, S., A. Abbosh, and M. A. Antoniadis, "Compact CPW-fed planar monopole antenna with wide circular polarization bandwidth," *IEEE Antennas and Wireless Propagation Letters*, Vol. 12, 1295–1298, Oct. 2013.
5. Chen, Q., H. Zhang, L.-C. Yang, B. Xue, and X.-L. Min, "Broadband CPW-fed circularly polarized planar monopole antenna with inverted L-strip and asymmetric ground plane for WLAN application," *Progress In Electromagnetics Research C*, Vol. 74, 91–100, 2017.
6. Chen, T., J. Zhang, and W. Wang, "A novel CPW-fed planar monopole antenna with broadband circularly polarization," *Progress In Electromagnetics Research M*, Vol. 84, 11–20, 2019.
7. Chaudhary, P. and A. Kumar, "Compact ultra-wideband circularly polarized CPW-fed monopole antenna," *AEU — International Journal of Electronics and Communications*, Vol. 107, 137–145, 2019.
8. Sam, K. U. and P. Abdulla, "Truncated circular microstrip ultra wideband antenna exhibiting wideband circular polarization," *Progress In Electromagnetics Research C*, Vol. 99, 111–122, 2020.
9. Kumar, A., S. Dwari, G. P. Pandey, B. K. Kanaujia, and D. K. Singh, "A high gain wideband circularly polarized microstrip antenna," *International Journal of Microwave and Wireless Technologies*, 1–10, Feb. 2020.
10. Kumar, M. and V. Nath, "Circularly polarized microstrip-line-fed antenna with rotated elliptical slot serving satellite communications," *Wireless Personal Communications*, Vol. 110, No. 3, 1443–1458, Feb. 2020.
11. Huang, H.-F. and B. Wang, "A simple V-shaped slot antenna with broadband circular polarization," *Progress In Electromagnetics Research Letters*, Vol. 67, 67–73, 2017.
12. Ellis, S. M., J. J. Kponyo, and A.-R. Ahmed, "A compact wideband circularly polarized L-slot antenna edge-fed by a microstrip feedline for C-band applications," *Progress In Electromagnetics Research Letters*, Vol. 65, 95–102, 2017.
13. Nosrati, M. and N. Tavassolian, "Miniaturized circularly polarized square slot antenna with enhanced axial-ratio bandwidth using an antipodal Y-strip," *IEEE Antennas and Wireless Propagation Letters*, Vol. 16, 817–820, 2016.
14. Kwame, O. G., G. Wen, Y. Huang, A. E. Ampoma, and W. Hu, "Broadband circularly polarized cross shaped slot antenna with an improved feedline," *Progress In Electromagnetics Research C*, Vol. 74, 141–149, 2017.
15. Zhang, Y.-X., Y.-C. Jiao, H. Zhang, and Y. Gao, "A simple broadband flat-gain circularly polarized aperture antenna with multiple radiation modes," *Progress In Electromagnetics Research*, Vol. 81, 1–10, 2018.
16. Wu, Z., G. M. Wei, X. Li, and L. Yang, "A single-layer and compact circularly polarized wideband slot antenna based on "bent feed"," *Progress In Electromagnetics Research Letters*, Vol. 72, 39–44, 2018.
17. Chen, Q., H.-L. Zheng, T. Quan, and X. Li, "Broadband CPW-fed circularly polarized antenna with equiangular tapered-shaped feedline for ultra-wideband applications," *Progress In Electromagnetics Research C*, Vol. 26, 83–95, 2012.
18. Shokri, M., V. Rafii, S. Karamzadeh, Z. Amiri, and B. Virdee, "Miniaturised ultra-wideband circularly polarized antenna with modified ground plane," *Electronic Letters*, Vol. 50, No. 24, 1786–1788, Nov. 2014.
19. Kumar, S., K. W. Kim, H. C. Choi, S. Saxena, R. Tiwari, M. K. Khandelwal, S. K. Palaniswamy, and B. K. Kanaujia, "A low profile circularly polarized UWB antenna with integrated GSM band for wireless communication," *AEU — International Journal of Electronics and Communications*, Vol. 93, 224–232, Jun. 2018.
20. Bhanu Pratap, L., D. Kundu, and A. Mohan, "Planar microstrip-fed broadband circularly polarized antenna for UWB applications," *Microwave and Optical Technology Letters*, Vol. 58, No. 5, 1088–1093, May 2016.
21. Li, T., F.-S. Zhang, F. Gao, and Y.-L. Guo, "CPW-fed circularly polarized square slot antenna with enhanced bandwidth and reduced size for wideband wireless applications," *Progress In Electromagnetics Research C*, Vol. 65, 121–129, 2016.

22. Prakash, K. C., P. V. Vinesh, M. Mani, S. Mathew, P. Mohanan, and K. Vasudevan, "Printed circularly polarised asymmetric ultra-wideband antenna," *Progress In Electromagnetics Research M*, Vol. 74, 179–189, 2018.
23. Kumar, G. and K. P. Ray, *Broadband Microstrip Antennas*, Artech House, Norwood, MA, 2003.
24. Balanis, C. A., *Antenna Theory: Analysis and Design*, John Wiley & Sons, Inc., 2005.
25. Brist, G. and G. Long, "Advanced print circuit board materials," *Materials for Advanced Packaging*, 273–306, Springer, Boston, MA, 2009.
26. Mumby, S. J. and J. Yuan, "Dielectric properties of FR-4 laminates as a function of thickness and the electrical frequency of the measurement," *Journal of Electronic Materials*, Vol. 18, No. 2, 287–292, 1989.
27. Mumby, S. and J. Yuan, "Dielectric properties of FR-4 laminates as a function of thickness and the electrical frequency of the measurement," *Journal of Electronic Materials*, Vol. 18, 287–292, 1989.
28. Paul, L. C., M. S. Hosain, S. Sarker, M. H. Prio, M. Morshed, and A. K. Sarkar, "The effect of changing substrate material and thickness on the performance of inset feed microstrip patch antenna," *American Journal of Networks and Communications*, Vol. 4, No. 3, 54–58, 2015.
29. Natarajan, D. and V. Chatterjee, "Effect of substrate permittivity and thickness on performance of single-layer, wideband, U-slot antennas on microwave substrates," *20th Annu. Rev. Prog. Appl. Comput. Electromagn.*, Vol. 7, 2004.